Ahmad, Saeed; Ding, Er-Xiong; Zhang, Qiang; Jiang, Hua; Sainio, Jani; Tavakkoli, Mohammad; Hussain, Aqeel; Liao, Yongping; Kauppinen, Esko I.

# Roles of sulfur in floating-catalyst CVD growth of single-walled carbon nanotubes for transparent conductive film applications

*Published in:*
Chemical Engineering Journal

*DOI:*
10.1016/j.cej.2019.122010

Published: 15/12/2019

*Document Version*
Peer-reviewed accepted author manuscript, also known as Final accepted manuscript or Post-print


# Roles of sulfur in floating-catalyst CVD growth of single-walled carbon nanotubes for transparent conductive film applications

Saeed Ahmad, Er-Xiong Ding, Qiang Zhang, Hua Jiang, Jani Sainio, Mohammad Tavakkoli, Aqeel Hussain, Yongping Liao, Esko I. Kauppinen

PII: S1385-8947(19)31404-4
DOI: https://doi.org/10.1016/j.cej.2019.122010
Article Number: 122010
Reference: CEJ 122010

To appear in: *Chemical Engineering Journal*

Received Date: 24 April 2019
Revised Date: 13 June 2019
Accepted Date: 17 June 2019

Please cite this article as: S. Ahmad, E-X. Ding, Q. Zhang, H. Jiang, J. Sainio, M. Tavakkoli, A. Hussain, Y. Liao, E.I. Kauppinen, Roles of sulfur in floating-catalyst CVD growth of single-walled carbon nanotubes for transparent conductive film applications, *Chemical Engineering Journal* (2019), doi: https://doi.org/10.1016/j.cej.2019.122010

# Roles of sulfur in floating-catalyst CVD growth of single-walled carbon nanotubes for transparent conductive film applications

Saeed Ahmad, Er-Xiong Ding, Qiang Zhang*, Hua Jiang, Jani Sainio, Mohammad Tavakkoli, Aqeel Hussain, Yongping Liao and Esko I. Kauppinen*

Department of Applied Physics, Aalto University School of Science, P.O. Box 15100, FI-00076 Aalto, Finland.

**Abstract**

Sulfur is an effective promoter for growing single-walled carbon nanotubes (SWCNTs) and tuning their structural properties. In particular, sulfur has been utilized in the floating-catalyst chemical vapor deposition (FC-CVD) process to fabricate SWCNT-based transparent conductive films (TCFs). However, *in-situ* catalyst nucleation process in conventional FC-CVD, hinders to correlate the substantial role of sulfur in tuning SWCNTs synthesis and enhancing the performance of SWCNT-based TCFs. Herein, we have for the first time, systematically studied the roles of sulfur on yield, morphology, and structure of SWCNTs grown by FC-CVD, using *ex-situ* Fe and Co catalyst particles. We found that SWCNT yield is largely dependent on the amount of sulfur introduced into the FC-CVD reactor and on catalyst composition. More importantly, the addition of an optimized amount of sulfur resulted in a three-fold enhancement of the opto-electronic performance of SWCNT-TCFs, by increasing diameter and bundle length along with improving the quality of SWCNTs. Surprisingly, electron diffraction analysis revealed that SWCNTs grown

* Corresponding author.
E-mail addresses: esko.kauppinen@aalto.fi (Esko I. Kauppinen), qiang.zhang@aalto.fi (Qiang Zhang)

from both Fe and Co display wide chirality distributions spanning from zig-zag to armchair edges, indicating that the sulfur promoter has little influence on the chirality modulating of SWCNTs.

**Keywords**

Floating-catalyst, single-walled carbon nanotubes, growth promoter, electron diffraction.

## 1. Introduction

Transparent conducting films (TCFs) are critical components for many modern optoelectronic devices [1,2]. In general, the core materials for TCFs applications must have high electrical conductivity and optical transmittance. Indium tin oxide (ITO) has excellent opto-electronic properties and is the most widely used TCF material. However, the brittle nature [3] and limited supply [2] of ITO limit its potential for application in next generation flexible electronics. Single-walled carbon nanotube (SWCNT) films, with a low refractive index [4], excellent mechanical flexibility, low haze [5] and optical transparency [6], are one of the most promising materials for the replacement of ITO as TCFs in future flexible electronics. However, SWCNT-TCFs have lower conductivity than commercial ITO. Therefore, substantial recent efforts [6–8] have been devoted to improving the performance of SWCNT-TCFs.

To date, two main types of process, solution-based purifications [4,5] or direct gas-phase production [6,7], have been used for SWCNT-TCF fabrication. The direct gas-phase production method is more straightforward and better preserves the inherent properties of SWCNTs than solution-based purification, in which SWCNTs are needed to disperse in solution. Specifically, the floating-catalyst chemical vapor deposition (FC-CVD) technique, a continuous, scaleable, single-step method, has been extensively employed to produce high performance SWCNT-TCFs [7,8].

Sulfur is one of the most important growth promoter in SWCNT synthesis by FC-CVD for fabricating SWCNT-TCFs [8–11]. However, the concrete impacts of sulfur addition on the yield, morphology and structure of SWCNTs, and on the performance of the SWCNT-based films, remain ambiguous. Since, in most of the cases without sulfur, no information about SWCNT yield, morphology, structure and also the performance of the SWCNTs based films has been provided. In some cases, however, it has been reported that SWCNTs are not formed at all without sulfur [9]. Moreover, in all the reported works, the sulfur source has been added simultaneously with the catalyst precursor to the FC-CVD reactor [8–12], which makes it complicated to investigate the independent role of sulfur addition. Because in the presence of catalyst-precursor pyrolysis, sulfur can affect catalyst formation at the nucleation stage resulting in changes to their composition and morphology. On the other hand, in supported-CVD methods with sulfur as a promoter, the chiral structure and metallic to semiconducting ratio of SWCNTs have been found highly dependent on catalyst composition [13,14]. To gain a more profound understanding of the role of sulfur as a promoter, it is necessary to be able to control sulfur addition during SWCNT synthesis by FC-CVD.

In this work, we have systematically investigated the roles of sulfur on various growth profiles (i.e. yield, diameter, bundle length and chirality) of SWCNTs, which influence the performance of SWCNT-TCFs. To be able to avoid above mentioned *in-situ* growth constraints, we have decoupled catalyst particle formation from the SWCNT growth process. Catalyst particles were pre-produced in an *ex-situ* spark discharge generator (SDG) through physical evaporation of the electrode's material [15]. The catalyst particles, along with ethylene, were then introduced into the FC-CVD reactor for SWCNT synthesis. A certain amount of $H_2S$ was added as a growth promoter to the FC-CVD reactor to tune SWCNT growth. $H_2S$ served as a sulfur source to make

synthesis process well-controlled and purely in gas-phase. To explore the effect of catalyst composition on sulfur-assisted FC-CVD, two different catalysts (Fe and Co) were utilized. We found that SWCNT yield is highly dependent on sulfur concentration and catalyst composition. We also demonstrated that, for both catalysts, an appropriate amount of sulfur can increase bundle length, SWCNT diameter and quality, and thus significantly enhance the performance of SWCNT-TCFs. Furthermore, comprehensive electron diffraction analyses of Fe-SWCNTs and Co-SWCNTs revealed that sulfur has no significant effect on the chirality distributions of SWCNTs produced by FC-CVD. This differs from early reports on the supported-CVD growth process [13,14]. Our work provides new insights into the fundamental mechanisms behind the sulfur-assisted FC-CVD growth of SWCNTs, and thus opens up new prospects for structure-controlled growth of SWCNTs and for their future applications as TCFs in modern nanoscale device technology.

## 2. Experimental section

### 2.1 Synthesis of catalyst particles

Catalyst particles were synthesized inside a rod-to-tube type spark discharge generator (SDG) [15]. Briefly, highly pure Fe (99.8%) or Co (99.95%) rod and tube electrodes were used as a source of catalyst particles to produce Fe-SWCNT and Co-SWCNT samples. Materials from the electrodes were evaporated by applying a high voltage on the order of a few (2-3) kV across the electrode gap in the presence of carrier gas ($N_2$ 99.995%). Catalyst particles were synthesized through the evaporation-nucleation-condensation process and they were carried from the SDG to the FC-CVD reactor by $N_2$.

### 2.2 Synthesis of SWCNTs

SWCNTs were synthesized in a vertical FC-CVD reactor using spark-produced Fe and Co catalyst particles with ethylene (99.999%, AGA) as the carbon source [16]. A schematic of the FC-CVD reactor is provided in the supporting information (Fig. S1). SWCNTs were synthesized using 0.1 sccm (200 ppm) ethylene and 80 sccm $H_2$ (99.999%, AGA) at a set furnace temperature of 1050 $^oC$. Diluted $H_2S$ (0.01vol. % $H_2S$ in $N_2$, 99.999%, AGA) in the flow range of 0-50 sccm (corresponding to 0-10 ppm $H_2S$ concentration) was employed as a source of sulfur. Catalyst particles were introduced into the FC-CVD reactor by 420-370 sccm $N_2$ flow from the SDG. The flow of $N_2$ from the SDG containing the catalyst particles and that of 0.01% diluted $H_2S$ were adjusted to keep total flow (500 sccm) and residence time constant. At the outlet of the FC-CVD reactor, as-grown SWCNTs were collected on an MF-Millipore membrane filter (13mm diameter Merck Millipore; France) in the form of a thin film for their optical characterization. The films were directly transferred onto transparent quartz slides by the dry press-transfer technique [7]. For electron microscopy, SWCNTs were deposited directly onto a TEM copper grid, or onto a $Si/SiO_2$ substrate via the thermophoresis deposition method [17]. SWCNT thin films were doped by a drop-casting technique using a 16 mM solution of $AuCl_3$ (99.99%, Sigma-Aldrich) in acetonitrile ($C_2H_3N$) [18]. After doping, films were washed with pure $C_2H_3N$ and dried with $N_2$ before the measurement of sheet resistances.

### 2.3. Characterizations

#### 2.3.1 Measurement of catalyst and CNT number concentration in gas-phase

Before feeding catalyst particles into the FC-CVD reactor, their number concentration (NC) and size were measured with a differential mobility analyzer (DMA) (SMPS+FCE, the GRIMM Aerosol Technic GmbH, Germany). To eliminate the effect of catalyst particles size and NC on

SWCNTs, we fixed their average size to ~3.5 nm with a total NC of ~$4.3\times10^6$ $cm^{-3}$. The effect of $H_2S$ concentration on the NC of SWCNTs in gas-phase was monitored by DMA.

### 2.3.2 Optical characterizations and yield calculation

For optical characterizations of SWCNTs, UV-Vis-NIR and Raman spectroscopy techniques were employed. Optical absorption spectra (OAS) of SWCNTs in the wavelength range of 200-2500 nm and transmittance (%) (at 550 nm wavelength) were measured using a UV-Vis-NIR spectrometer (Agilent Carry 5000; Agilent Technologies, Inc.). A Raman spectrometer (Horiba Labram-HR 800; Horiba Jobin-Yvon) was used to acquire Raman spectra of SWCNTs by three different excitation lasers (488, 514 & 633 nm).

The SWCNT yield was calculated based on the transmittance of the as-produced film. For a fixed time and collection area, film thickness depends on SWCNT yield. Film thickness is related to transmittance by the Beer–Lambert law, $L \propto -lnT$ (where, $L$ is film thickness and $T$ is transmittance). Therefore, we can utilize the optical transmittance of the film to obtain the normalized yield of SWCNTs. The yield was quantified by collecting samples on a membrane filter (13 mm diameter) with different $H_2S$ concentrations for a fixed time (3 hrs).

### 2.3.3 Electron microscopy characterizations

The bundle lengths of SWCNTs produced under different synthesis conditions were compared by scanning electron microscopy (Zeiss Sigma VP; Carl Zeiss GmbH, Germany). The catalyst particle size, and the bundle diameter distributions and electron diffraction (ED) of SWCNTs were measured using a double aberration-corrected high-resolution transmission electron microscope (HR-TEM) (JEOL-2200FS; JEOL Ltd., Japan).

### 2.3.4 X-ray photoelectron spectroscopy of SWCNT films

Elemental analysis of sulfur-assisted SWCNT films was carried out by using a Kratos Axis Ultra spectrometer with monochromated Al $K_{\alpha}$-radiation, a pass energy of 40 eV, X-ray power of 225 W and an analysis area of approximately $700\ \mu m \times\ 300\ \mu m$.

### 2.3.5 Sheet resistances of SWCNT films

Sheet resistances of SWCNT-TCFs were measured using a Jandel 4-point probe (Jandel Engineering Ltd; UK) combined with a multi-meter (HP/Hewlett Packard 3485A). SWCNT films with varying thickness were analyzed to allow comparisons of sheet resistance at different values of transmittance (%). Transmittance (%) versus sheet resistance values of the SWCNT films were nonlinearly fitted by fitting-method described elsewhere [7].

## 3. Results and discussions

Firstly, the growth process without adding $H_2S$ was kinetically optimized to produce SWCNTs. By kinetically optimized we mean the more suitable growth conditions including temperature of the FC-CVD reactor, number concentration of catalyst particles, amount of carbon source and flow rate of different gases in the FC-CVD reactor to acquire minimum sheet resistance of SWCNT-TCFs with 90% transmittance (@ 550 nm wavelength). For both Co and Fe catalysts, the highest conductivity of pristine SWCNT films was obtained with the synthesis parameters of 80 sccm $H_2$ and 0.1 sccm $C_2H_4$ (200 ppm). Then 0 to 10 ppm $H_2S$ was added into the FC-CVD reactor, and the effect of $H_2S$ on SWCNT growth was systematically studied (Fig. 1 and 2). For all the experiments, the total number concentration and mobility diameters of catalyst particles were fixed to ~4.3×106 $cm^{-3}$ and ~3.5 nm, respectively (Fig. S2). We found SWCNT yield to be highly sensitive to sulfur concentration. With an increase in the amount of $H_2S$, SWCNT yield first

increased and then started to decrease. The yield was quantified from the transmittance of as-produced SWCNT films. For different $H_2S$ concentrations the normalized yield was calculated relative to the yield at 0 ppm $H_2S$ (Fig. 1a). Adding an appropriate amount of sulfur resulted in a 2.5-fold increase in SWCNT yield. The optimum $H_2S$ concentration that was required to obtain this maximum yield was different for Fe and Co catalysts, i.e., 1 ppm for Fe- and 2 ppm for Co-SWCNTs. This indicates that the influence of sulfur on SWCNT growth is also dependent on catalyst composition. The addition of more $H_2S$ above these concentrations resulted in declining yields, meaning that excess $H_2S$ acts to suppress the yield. Therefore, excessive amount of $H_2S$ has negative effects on growth of SWCNTs as has been observed in the earlier studies [19]. For example, 10 ppm $H_2S$ resulted in a yield that was only ~15% of that with 0 ppm $H_2S$.

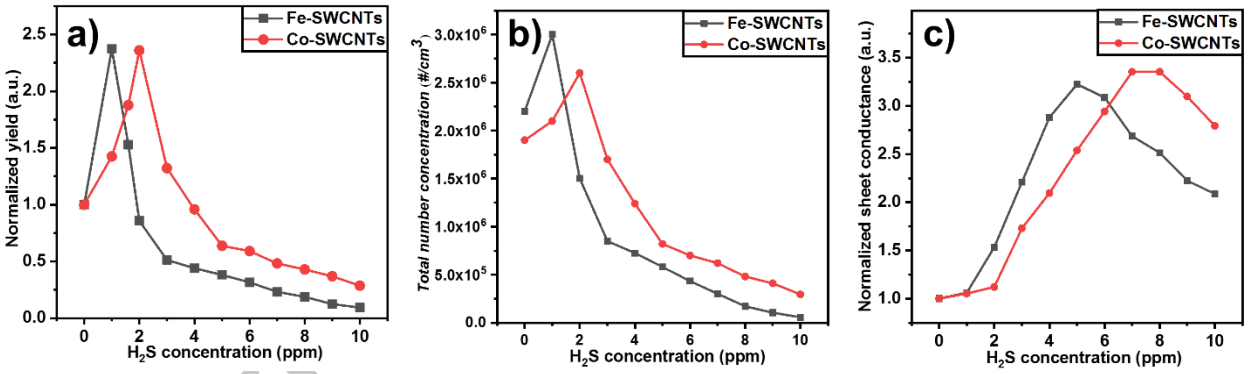


***Fig. 1. a)*** *Normalized yield obtained from optical transmittance data with Fe and Co as the catalyst.* ***b)*** *Total number concentration of Fe- and Co-SWCNTs monitored by DMA.* ***c)*** *Variation in the sheet conductance of pristine Fe-SWCNTs and Co-SWCNT films (at 90% transmittance for 550 nm wavelength) with increasing $H_2S$ concentration (0-10 ppm). Maximum sheet conductance was observed at 5 and 8 ppm $H_2S$ for Fe-SWCNTs and Co-SWCNTs, respectively.*

The total NC of SWCNTs as a function of $H_2S$ concentration (Fig. 1b and S3) followed a similar trend to that in yields. Total NC increased by ~37% with 1 ppm of $H_2S$ for Fe catalysts, and by ~34% with 2 ppm $H_2S$ for Co catalysts, relative to NC values at 0 ppm $H_2S$. However, further addition of $H_2S$ resulted in declining total NC values. With 10 ppm $H_2S$, there was a ~90% reduction in total NC for both Fe and Co catalysts, compared to values obtained without $H_2S$. This suggests that the sulfur addition tunes the proportion of active catalyst particles.

$H_2S$ addition noticeably increased the diameter of the SWCNTs. It can be seen in the optical absorption spectra (OAS) (Fig. 2a & b) of as-produced SWCNT films, the first inter-band transition peak in semiconducting nanotubes ($S_{11}$) shifts from 1322 nm to 1525 nm with 1 ppm $H_2S$ addition. The mean diameter of SWCNTs, calculated using Kataura plots and OAS, increased from 1.05 nm to 1.26 nm with $H_2S$ addition for both Fe and Co catalysts. However, from 2-10 ppm $H_2S$, no shift in $S_{11}$ was observed compared to 1 ppm $H_2S$, indicating that SWCNT diameter is not sensitive to the amount of $H_2S$ in the range 1 to 10 ppm. Poisoning of small catalyst particles by sulfur addition could be one of the possible reasons for the growth of large diameter nanotubes with sulfur addition.

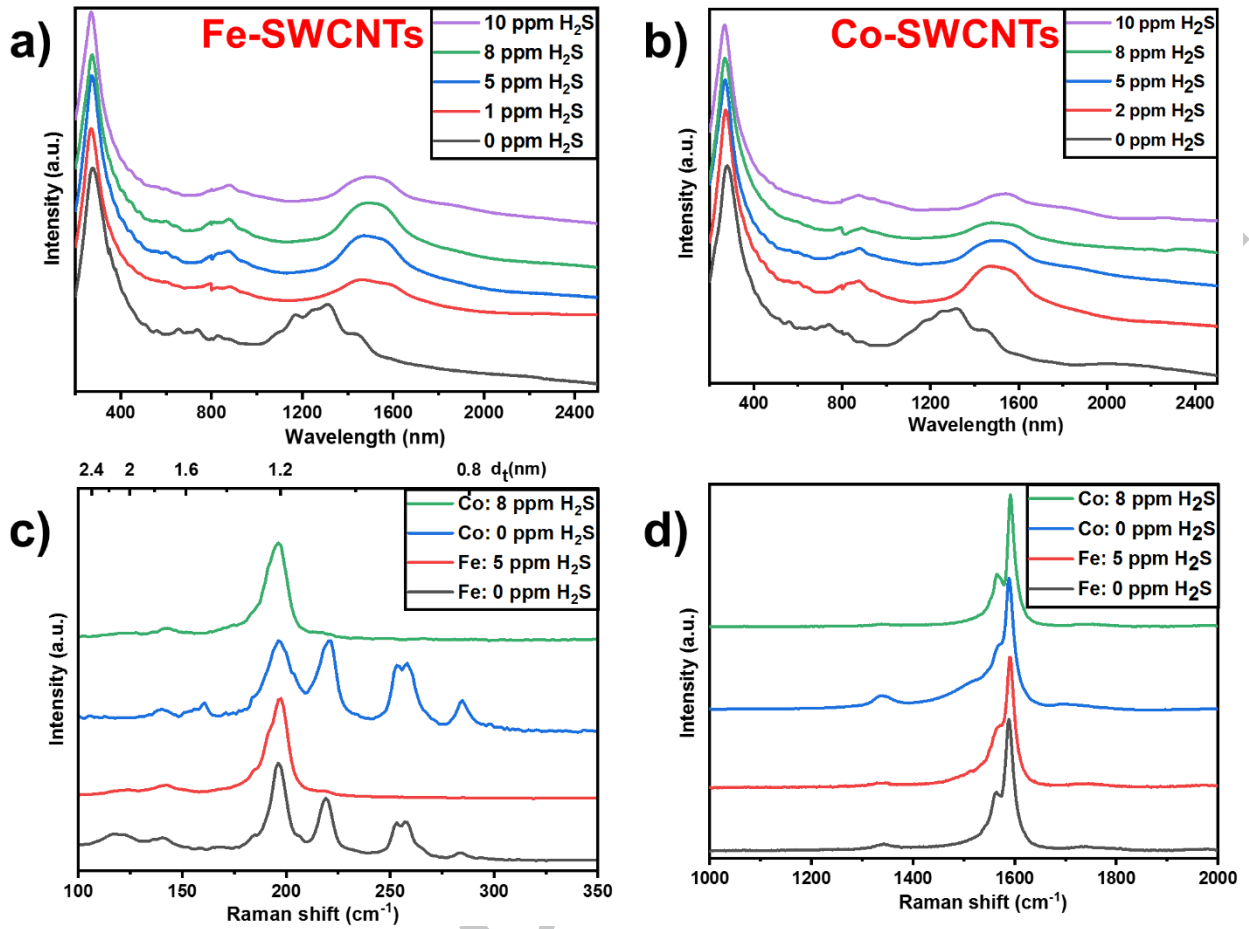


***Fig. 2.*** *The absorption spectra of* ***a)*** *Fe-SWCNTs and* ***b)*** *Co-SWCNTs indicate a very clear shift towards large diameter SWCNTs with $H_2S$ addition. Corresponding* ***c)*** *Radial breathing mode of Raman spectra with a 633 nm laser and* ***d)*** *the G and D mode of Raman spectra showing an increase in the $I_G/I_D$ ratio of 13 to 19 for Fe-SWCNTs and 11 to 21 for Co-SWCNTs.*

These results are also supported by Raman spectra of SWCNT films with three excitation lasers (633, 514 & 488 nm). Without the addition of $H_2S$, SWCNTs in resonance with the applied laser were in the 0.8-1.7 nm diameter range (Fig. 2c and Fig. S4). However, with addition of 1 to 10 ppm $H_2S$, only SWCNTs with a diameter ($d$) greater than 1.1 nm were detected. Furthermore, sulfur addition resulted in a conspicuous increase in the intensity of G mode compared to D mode in the Raman spectra (Fig. 2d and S4), indicating an enhancement in the quality of the SWCNTs.

Both yield variation and diameter increase of CNTs with sulfur addition have already been reported in the sulfur-assisted FC-CVD SWCNT growth process [20,21]. The mechanism proposed previously is that sulfur can change the size and composition of the catalysts by forming a sulfur-enriched layer on the catalyst surface. However, the *in-situ* catalyst formation makes the essential role of sulfur ambiguous. In our case, unlike in earlier studies [20,21], we did not observe significant change in either catalyst size or composition with $H_2S$ addition. We found that the size distribution of the catalyst particles, measured using HR-TEM micrographs, was fairly consistent with and without sulfur addition (Fig. S5c). The effect of sulfur on catalyst composition was explored by X-rays energy dispersive spectroscopy (EDS) and X-ray photoelectron spectroscopy (XPS) analysis. There was no detectable sulfur peak in the EDS spectrum of the Fe catalyst particles, suggesting that their composition is independent of sulfur (Fig. S5b). On the contrary, XPS analysis of SWCNT films (Fig. S6) revealed the presence of both iron (0.04 at. %) and sulfur (0.05 at. %) in the sample. The atomic concentrations of both Fe and S are of the order of the detection limit of XPS and thus their spectra have poor statistics (Fig. S6a and S6b). However, in the Fe 2p spectrum (Fig, S6a) two peaks can be observed roughly around 707 eV ($2p_{3/2}$) and 720 eV ($2p_{1/2}$) which would be consistent with metallic Fe. For sulfur, there are two broad S 2p features between 161-166 eV and 167-171 eV (Fig. S6b). For the lower energy feature several chemical states are possible, including S-S bonding and C-S bonding, whereas the higher binding energy feature could be related e.g. to C-$SO_x$-type bonding [22–24]. Iron sulfide or sulfur-containing iron alloys should be observed at S 2p binding energies between 161-163 eV [22,25] and thus this does not seem to be the majority sulfur species on the surface. Thermodynamically, $H_2S$ can easily adsorb onto the surface of catalyst particles and decompose into activated fragments like -SH and –H [26–28]. These activated species on catalysts might promote carbon-catalyst interface bonding

[29] as has been indicated by C-S type bonding in our XPS spectrum, resulting in more active catalyst sites and longer SWCNTs, as well as an increase in yield. Moreover, large localized active regions on the catalyst particle with sulfur addition could induce the formations of large carbon cap and large diameter SWCNTs accordingly [21,29,30]. Therefore, we propose that $H_2S$ mainly influences the interaction between the metal catalyst and carbon. On the other hand, an excess of sulfur may lead to an imbalance between carbon dissolution and precipitation, which can decrease catalyst activity and even deactivate the catalysts. Therefore, with excessive $H_2S$, yields will decline.

More importantly, we found that $H_2S$ can effectively tune the conductivity of the as-produced SWCNT films. SWCNT film conductivity initially increases and then decreases with an increase in $H_2S$ (Fig 1c). For both catalysts (Fe and Co), the conductivity of pristine SWCNT films can be drastically increased, by a factor of three, with sulfur addition. The optimum $H_2S$ concentration for maximum sheet conductance with Fe as the catalyst was 5 ppm whereas that for Co was 8 ppm. To understand the mechanism by which sulfur improves the conductivity of SWCNT films, we studied in detail the morphology and structure of as-produced SWCNTs with and without $H_2S$ addition at optimum conditions.

The diameter distribution and geometric mean diameter ($\mu_g$) of the SWCNTs were quantified by ED [31]. For this purpose, 115-125 individual SWCNTs were randomly selected from each sample and characterized. The ED analysis results are plotted as diameter distributions in Figs. 3a and 3b for Fe- and Co-SWCNTs, respectively. The $\mu_g$ for Fe-SWCNTs increased from 1.06 nm to 1.26 nm with the addition of 5 ppm $H_2S$. The geometric standard deviation ($б_g$) decreased from 1.23 to 1.17, indicating a narrower diameter distribution with $H_2S$ addition. The

smallest diameter SWCNTs with $H_2S$ were ≈ 0.95 nm compared to diameters ≈ 0.70 nm without $H_2S$. For Co-SWCNTs, the $\mu_g$ increased from 1.05 nm to 1.24 nm with the addition of 8 ppm $H_2S$, and the diameter distribution became broader with $H_2S$ addition. The formation of large diameter nanotubes with a small band gap after sulfur addition is a major explanation for the improved conductivity of the resulting SWCNT films.

Our previous work has shown that bundle length and bundle diameter both have a pronounced effect on the opto-electronic performance of SWCNT films.[6,10] Therefore, we explored the effect of sulfur addition on the bundle length and bundle diameter of SWCNTs. It is worth noting that in the existing literature, the reported outcome when no sulfur was added has been either no CNTs or very short CNTs [9,32,33] precluding comparisons of bundle length distributions with and without sulfur addition. However, we measured the bundle length of SWCNTs with and without sulfur addition and a typical SEM image utilized for the said purpose is shown in Fig.4a. For statistical analysis, the bundle length distribution of 200-220 SWCNT bundles with Fe or Co as the catalyst, and with and without sulfur addition was measured and has been shown in Fig. 4b and c. We found that the average bundle length ($l_b$) of Fe-SWCNTs increased by 25% (from 3.4 μm to 4.2 μm) with the addition of 5 ppm $H_2S$ and a similar result for Co-SWCNTs was obtained by adding 8 ppm $H_2S$. As mentioned above, sulfur may reduce carbon precipitation from catalysts and increase the growth rate of SWCNTs, producing longer SWCNT bundles. For TCF applications, at the same transmittance, nanotubes with longer bundle lengths show better performance due to lower number of contact junctions, hence improving the overall opto-electronic performance of the resulting films.

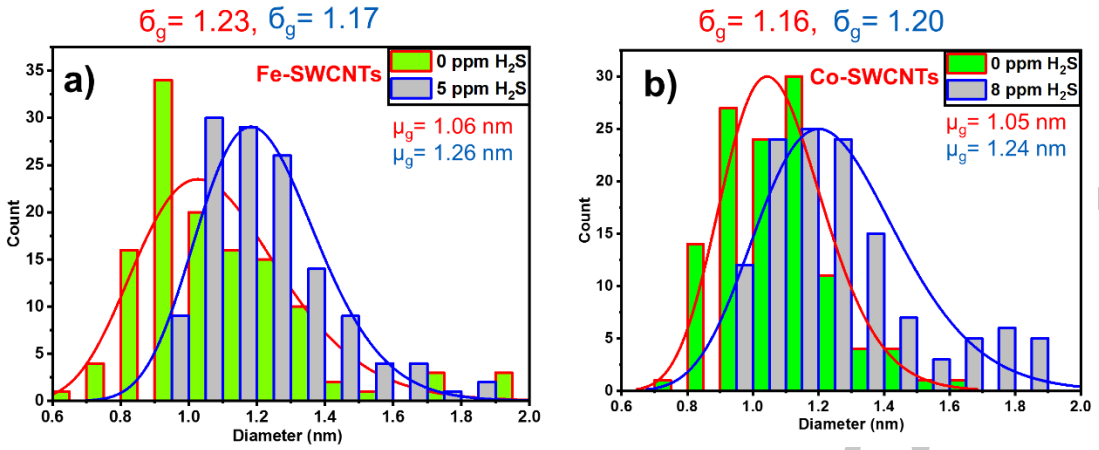


***Fig. 3.*** *Quantitative analysis of SWCNT diameter distributions at optimized conditions measured by electron diffraction with and without $H_2S$ for* ***a)*** *Fe-SWCNTs and* ***b)*** *Co-SWCNTs.*

To investigate the effect of sulfur on bundle diameter distributions, we acquired 170-190 HR-TEM images of SWCNTs with and without sulfur addition. Fig. 4d shows a typical HR-TEM image of an individual and a bundled SWCNT. The bundle diameter distributions are provided in Figs 4e and f for Fe and Co-SWCNTs, respectively. We observed an increase in the amount of individual Fe-SWCNTs from 13% to 21%, and for Co-SWCNTs from 11% to 18%, with sulfur addition. Sulfur addition also reduced mean bundle diameter $(d_b)$ for Fe-SWCNTs by 0.5 nm and for Co-SWCNTs by 0.7 nm. More importantly, the number of SWCNTs in an average-sized bundle declined from 9 to 5 for Fe-SWCNTs with the introduction of 5 ppm $H_2S$, and from 12 to 5 for Co-SWCNTs with the addition of 8 ppm $H_2S$ (insets in Fig. 4e and f). In bundled nanotubes, the charge is carried by the outermost nanotubes [6] and nanotubes inside the bundle mainly contribute to light absorption rather than charge transportation. Therefore, SWCNT films comprised of narrower bundles with a higher fraction of individual nanotubes could exhibit better opto-electronic performance.

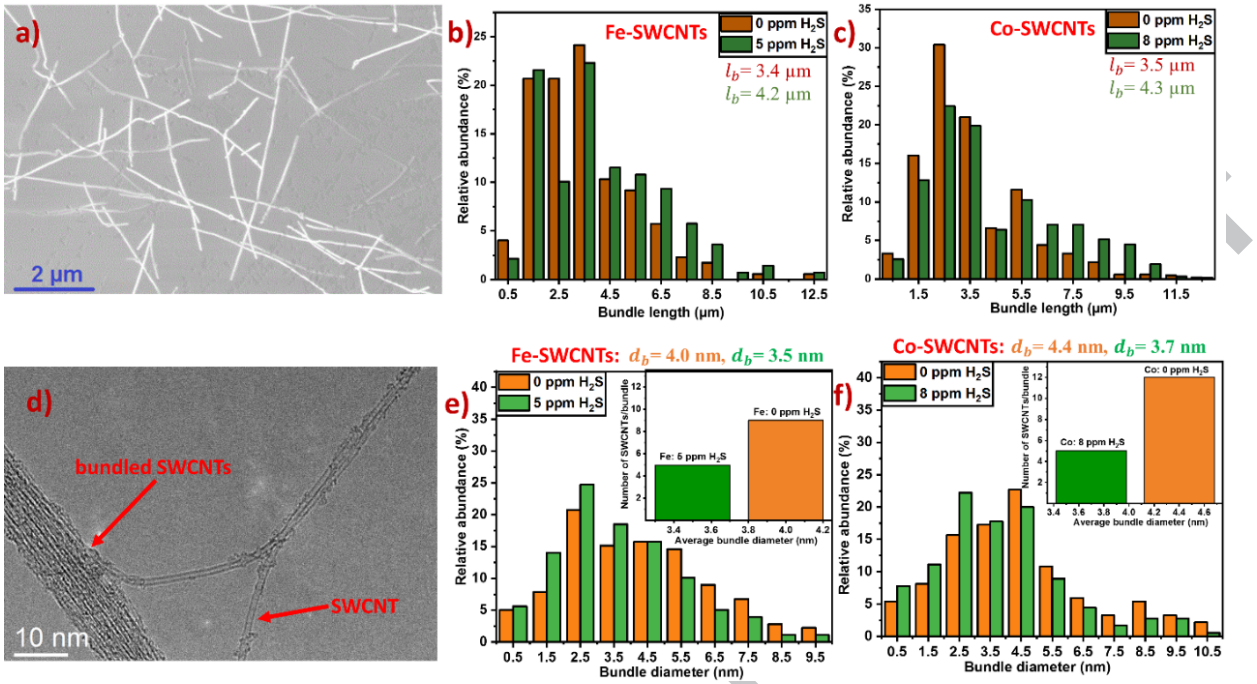


***Fig. 4. a)*** *A typical SEM image of SWCNTs used for bundle length measurement. A comparison of the bundle length distribution of SWCNTs with* ***b)*** *Fe (at 0 and 5 ppm $H_2S$) and* ***c)*** *Co (at 0 and 8 ppm $H_2S$) catalysts.* ***d)*** *HR-TEM image, showing a bundled and an individual SWCNT. A comparison of bundle diameter distribution and, in the inset, the number of SWCNTs required to form the average bundle size of* ***e)*** *Fe-SWCNTs (at 0 and 5 ppm $H_2S$) and* ***f)*** *Co-SWCNTs (at 0 and 8 ppm $H_2S$).*

The chirality, i.e. atomic structure of nanotubes, plays a critical role for their applications including the TCFs. To determine chirality of SWCNTs, we utilized the highly reliable and precise ED technique [31,34]. To the best of our knowledge, this is the first report on the effect of sulfur addition on SWCNTs chirality distributions obtained from ED. Previously, the challenge of synthesizing of high-quality and clean SWCNTs without sulfur addition has hindered this comparison. Earlier determination of SWCNT chiralities has been based on absorption, Raman and photoluminescence spectroscopy, among which Raman and photoluminescence techniques

have serious drawbacks, leading to the incomplete chirality maps [34]. Chirality maps of Fe-SWCNTs and Co-SWCNTs based on ED are shown in Fig. 5, and selected ED patterns are provided in the supporting information (Fig. S7). ED analysis revealed that the chirality distributions of Fe-SWCNTs for both 0 and 5 ppm $H_2S$ were randomly distributed from zig-zag to armchair edges. The most abundant chiralities without $H_2S$ addition were (8, 6), (9, 5) and (10, 4), representing 12% of the total nanotubes.

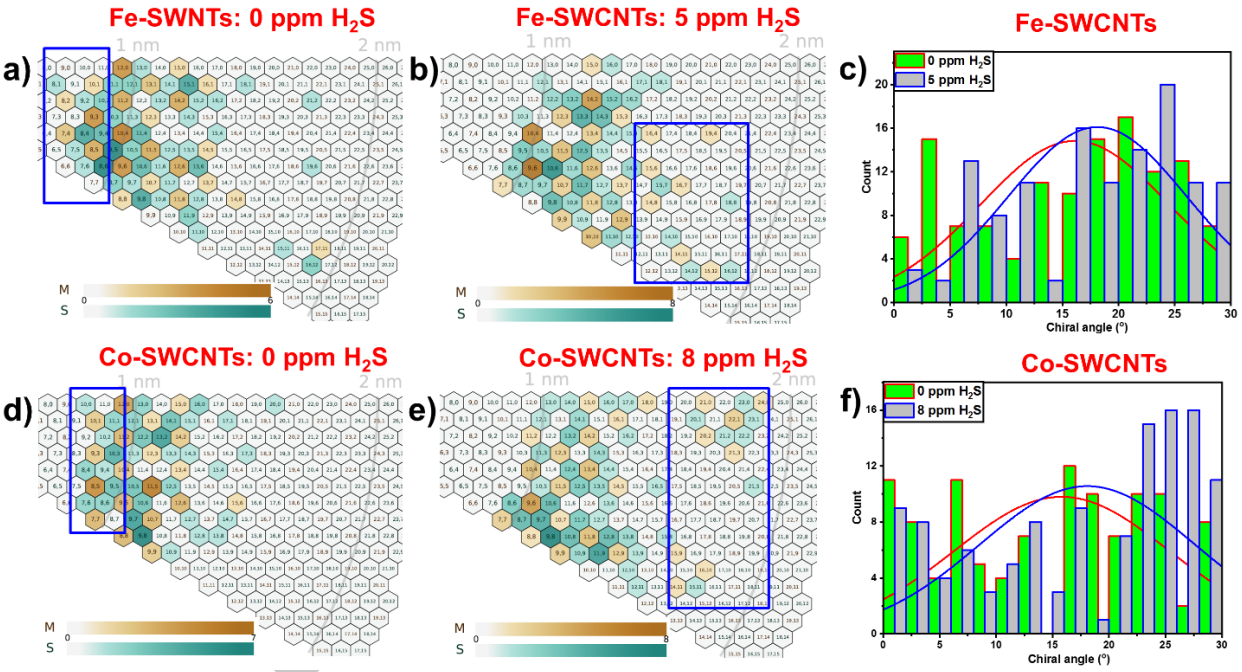


***Fig.5.*** *Chirality maps of SWCNTs obtained by electron diffraction with* ***a)*** *Fe 0 ppm $H_2S$,* ***b)*** *Fe 5 ppm $H_2S$,* ***d)*** *Co 0 ppm $H_2S$, and* ***e)*** *Co 8 ppm $H_2S$. A comparison of the change in chiral angle with the addition of $H_2S$ for* ***c)*** *Fe-SWCNTs and* ***f)*** *Co-SWCNTs.*

In the chirality map (Fig. 5a) with 0 ppm $H_2S$, most of the nanotubes were clustered around the 1 nm region with 45% having $d < 1$ nm. However, with the addition of 5 ppm $H_2S$ nanotubes with $d < 0.95$ nm, which are enclosed in the rectangle in Fig. 5a, disappeared completely. With 5 ppm $H_2S$, 17% of the nanotubes had chiralities (9, 6), (10, 6) and (10, 4). Some large diameter

nanotubes, for example (16, 4), (16, 10) and (18, 8), were only found with the addition of $H_2S$ (Fig. 5b). More importantly, sulfur did not play a significant role in tuning the chiral angle distribution (Fig. 5c). Only a modest increase in the mean chiral angle from 16.06±8.35° to 18.11±7.92° was observed with $H_2S$ addition. Moreover, the ratio of semiconducting tubes slightly declined from 61% to 59% with $H_2S$ addition.

A similar trend was found in Co-SWCNTs. The most abundant chiralities (15%) for the Co catalyst with 0 ppm $H_2S$ were (9, 8), (9, 7), (11, 5), and 35% of the SWCNTs had $d < 1$ nm. With the addition of 8 ppm $H_2S$, the smallest nanotube diameter was 0.95 nm and the three most abundant chiralities (16% of nanotubes) were (9, 7), (9, 8) and (11, 5). The major changes in $(n,m)$ indices with 0 and 8 ppm $H_2S$, indicating shifts in chirality are highlighted with the rectangles in Fig. 5d and e. More detailed statistics on individual chirality are in the supporting information (Fig. S8-S11). It is worth noting that for the Co catalyst the addition of sulfur resulted in a relatively higher fraction (8%) of zig-zag $(n,0)$ nanotubes, which are considered to be more difficult to synthesize due to their comparatively slower growth rate owing to their symmetric structures.[35–37] But as a whole, similar to Fe-SWCNTs, we did not find any noticeable change in the mean chiral angle (Fig. 5f) or much change in the ratio of semiconducting (semiconducting ratio increased from 61% to 66%) Co-SWCNTs with the addition of sulfur. Hence, the ED results showed that for both catalysts (Fe and Co) there was a shift from smaller to larger diameter SWCNTs but no effective chirality control with the addition of sulfur. This result contrasts with those of many earlier studies on supported-CVD processes, where sulfur-containing compounds have been used as a promoter to gain high selectivity and to tune the metallic to semiconducting ratio of the SWCNTs [13,14]. This discrepancy may arise from the use of inadequate

characterization techniques for chirality determination, including Raman and photoluminescence spectroscopy, in earlier studies [34].

To summarize the analyses above, we found that an appropriate amount of sulfur increases the diameter of SWCNTs, elongates the bundle length, reduces the bundle size and enhances quality of the nanotubes, which can give rise to SWCNT films with a better opto-electronic performance. The plots of sheet resistance ($R_s$) versus transmittance (T) are shown in Fig. 6a to compare the opto-electronic performance of SWCNT-TCFs produced with and without $H_2S$. The result were non-linearly fitted by the well-established fitting method described in the literature [7]. For pristine Fe-SWCNT and Co-SWCNT films with 0 ppm $H_2S$ at 90% $T_{550\ nm,}$ sheet resistance values ($R_s$) were 1512 Ω/sq. and 1704 Ω/sq., respectively.

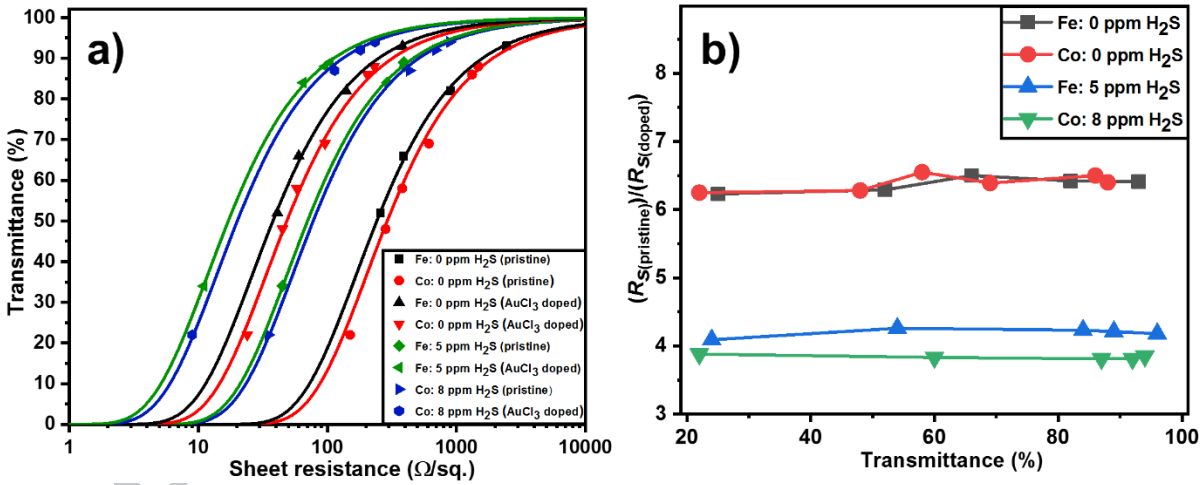


***Fig.6. a)*** *A comparison of sheet resistance versus % transmittance at 550 nm of SWCNT-TCFs under optimized conditions with and without sulfur addition, and before and after doping with* $AuCl_3$. ***b)*** *A reduction in the doping ratio of Fe-SWCNTs and Co-SWCNTs with sulfur addition at various % transmittance of the films.*

The conductivity of the pristine SWCNT films increased ~6 times when they were doped with $AuCl_3$. For doping, $AuCl_3$ was employed because previous studies indicated this to be a relatively stable dopant for SWCNTs [18,38]. The doped Fe and Co-SWCNT films had $R_s$ 243 Ω/sq. and 274 Ω/sq. at 90% $T_{550\ nm}$, respectively.

However, at optimized conditions with sulfur addition, the $R_s$values for pristine films remarkably reduced by a factor of ~3 for both Fe (469 Ω/sq. @ 90% $T_{550\ nm}$) and Co (508 Ω/sq. @ 90% $T_{550\ nm}$) SWCNTs. The reduction in $R_s$ with sulfur addition is mainly attributed to large diameter nanotubes, long bundle length and small bundle size. This enhancement in the quality ($I_G/I_D$) of SWCNTs with sulfur might also contribute in improving film performance. More importantly, after doping $R_s$value of sulfur-assisted pristine films decreased by a factor of ~4. It's worth noting here, that the doping factor was reduced from ~6 to ~4 with sulfur addition (Fig. 6b). This difference can be ascribed to the small band gaps of large diameter nanotubes and to fewer contact junctions caused by longer bundle length with sulfur addition. The minimum $R_s$ value for Fe-SWCNTs at 90% $T_{550\ nm}$ with sulfur addition after doping was 116 Ω/sq. and that for Co-SWCNTs was 132 Ω/sq..

## 4. Conclusion

In this work, we have for the first time systematically studied the effects of sulfur on the growth characteristics of FC-CVD-synthesized SWCNTs using pre-made Fe and Co catalyst particles. We demonstrate that the yield of SWCNTs can be improved around 2.5 times by introducing an appropriate amount of sulfur as a growth promoter. The addition of sulfur promotes the growth of large diameter nanotubes, with the average diameter of the resulting SWCNTs increasing from 1 nm to 1.2 nm. Moreover, optimized sulfur addition can increase the conductivity

of SWCNTs films by 3 times, leading to excellent opto-electronic performance TCFs, with 116 Ω/sq. for Fe-SWCNTs and 132 Ω/sq. for Co-SWCNTs at 90% $T_{550\ nm}$, respectively. The performance enhancement of SWCNT films with the aid of the sulfur promoter is attributed to increases in SWCNT diameter, quality, average bundle length, and in the fraction of individual nanotubes. Interestingly, ED analysis revealed that the sulfur promoter has little influence on the chirality distribution of SWCNTs. Our results comprehensively explored the roles of sulfur as a promoter for the FC-CVD growth of SWCNTs and are of special interest for the synthesis of highly conductive SWCNTs thin films applications.

**Acknowledgements**

The research described here has received funding from European Union Seventh Framework Program under Grant Agreement No. 604472 (IRENA project), and the Aalto Energy Efficiency (AEF) Research Program through the MOPPI project. The research has also been partially supported by Academy of Finland via projects 286546 (DEMEC), and 292600 (SUPER) as well as by TEKES Finland via projects 3303/31/2015 (CNT-PV) and 1882/31/2016 (FEDOC). This work made use of the Aalto University Nano-microscopy Center (Aalto-NMC) premises. The authors thank Dr. Mirkka Jones for proof reading.

**References**

[1] R. Rao, C.L. Pint, A.E. Islam, R.S. Weatherup, S. Hofmann, E.R. Meshot, F. Wu, C. Zhou, N. Dee, P.B. Amama, J. Carpena-Nuñez, W. Shi, D.L. Plata, E.S. Penev, B.I. Yakobson, P.B. Balbuena, C. Bichara, D.N. Futaba, S. Noda, H. Shin, K.S. Kim, B. Simard, F. Mirri, M. Pasquali, F. Fornasiero, E.I. Kauppinen, M. Arnold, B.A. Cola, P. Nikolaev, S. Arepalli, H.-M. Cheng, D.N. Zakharov, E.A. Stach, J. Zhang, F. Wei, M.

Terrones, D.B. Geohegan, B. Maruyama, S. Maruyama, Y. Li, W.W. Adams, A.J. Hart, Carbon Nanotubes and Related Nanomaterials: Critical Advances and Challenges for Synthesis toward Mainstream Commercial Applications, ACS Nano. (2018) acsnano.8b06511. doi:10.1021/acsnano.8b06511.

[2] K. Ellmer, Past achievements and future challenges in the development of optically transparent electrodes, Nat. Photonics. (2012). doi:10.1038/nphoton.2012.282.

[3] L. Yu, C. Shearer, J. Shapter, Recent Development of Carbon Nanotube Transparent Conductive Films, Chem. Rev. (2016). doi:10.1021/acs.chemrev.6b00179.

[4] Z. Wu, Transparent, Conductive Carbon Nanotube Films, Science (80-. ). 305 (2004) 1273–1276. doi:10.1126/science.1101243.

[5] D.S. Hecht, D. Thomas, L. Hu, C. Ladous, T. Lam, Y. Park, G. Irvin, P. Drzaic, Carbon-nanotube film on plastic as transparent electrode for resistive touch screens, J. Soc. Inf. Disp. (2009). doi:10.17660/ActaHortic.2002.575.61.

[6] K. Mustonen, P. Laiho, A. Kaskela, T. Susi, A.G. Nasibulin, E.I. Kauppinen, Uncovering the ultimate performance of single-walled carbon nanotube films as transparent conductors, Appl. Phys. Lett. (2015). doi:10.1063/1.4932942.

[7] A. Kaskela, A.G. Nasibulin, M.Y. Timmermans, B. Aitchison, A. Papadimitratos, Y. Tian, Z. Zhu, H. Jiang, D.P. Brown, A. Zakhidov, E.I. Kauppinen, Aerosol-synthesized SWCNT networks with tunable conductivity and transparency by a dry transfer technique, Nano Lett. (2010). doi:10.1021/nl101680s.

[8] E.-X. Ding, H. Jiang, Q. Zhang, Y. Tian, P. Laiho, A. Hussain, Y. Liao, N. Wei, E.I.

Kauppinen, Highly conductive and transparent single-walled carbon nanotube thin films from ethanol by floating catalyst chemical vapor deposition, Nanoscale. (2017). doi:10.1039/C7NR05554D.

[9] O. Reynaud, A.G. Nasibulin, A.S. Anisimov, I. V. Anoshkin, H. Jiang, E.I. Kauppinen, Aerosol feeding of catalyst precursor for CNT synthesis and highly conductive and transparent film fabrication, Chem. Eng. J. (2014). doi:10.1016/j.cej.2014.06.082.

[10] E.X. Ding, Q. Zhang, N. Wei, A.T. Khan, E.I. Kauppinen, High-performance single-walled carbon nanotube transparent conducting film fabricated by using low feeding rate of ethanol solution, R. Soc. Open Sci. 5 (2018). doi:10.1098/rsos.180392.

[11] S. Jiang, P.X. Hou, M.L. Chen, B.W. Wang, D.M. Sun, D.M. Tang, Q. Jin, Q.X. Guo, D.D. Zhang, J.H. Du, K.P. Tai, J. Tan, E.I. Kauppinen, C. Liu, H.M. Cheng, Ultrahigh-performance transparent conductive films of carbon-welded isolated single-wall carbon nanotubes, Sci. Adv. (2018). doi:10.1126/sciadv.aap9264.

[12] T.S. Gspann, F.R. Smail, A.H. Windle, Spinning of carbon nanotube fibres using the floating catalyst high temperature route: Purity issues and the critical role of sulphur, Faraday Discuss. (2014). doi:10.1039/c4fd00066h.

[13] Y. Yuan, H.E. Karahan, C. Yildirim, L. Wei, Ö. Birer, S. Zhai, R. Lau, Y. Chen, Smart poisoning of Co/SiO2catalysts by sulfidation for chirality-selective synthesis of (9,8) single-walled carbon nanotubes, Nanoscale. 8 (2016) 17705–17713. doi:10.1039/c6nr05938d.

[14] Y. Yuan, L. Wei, W. Jiang, K. Goh, R. Jiang, R. Lau, Y. Chen, Sulfur-induced chirality changes in single-walled carbon nanotube synthesis by ethanol chemical vapor deposition

on a Co/SiO2catalyst, J. Mater. Chem. A. 3 (2015) 3310–3319. doi:10.1039/c4ta05917d.

[15] S. Ahmad, P. Laiho, Q. Zhang, H. Jiang, A. Hussain, Y. Liao, E.X. Ding, N. Wei, E.I. Kauppinen, Gas phase synthesis of metallic and bimetallic catalyst nanoparticles by rod-to-tube type spark discharge generator, J. Aerosol Sci. 123 (2018) 208–218. doi:10.1016/j.jaerosci.2018.05.011.

[16] S. Ahmad, Y. Liao, A. Hussain, Q. Zhang, E.X. Ding, H. Jiang, E.I. Kauppinen, Systematic investigation of the catalyst composition effects on single-walled carbon nanotubes synthesis in floating-catalyst CVD, Carbon N. Y. (2019). doi:10.1016/j.carbon.2019.04.026.

[17] P. Laiho, K. Mustonen, Y. Ohno, S. Maruyama, E.I. Kauppinen, Dry and Direct Deposition of Aerosol-Synthesized Single-Walled Carbon Nanotubes by Thermophoresis, ACS Appl. Mater. Interfaces. 9 (2017) 20738–20747. doi:10.1021/acsami.7b03151.

[18] K.K. Ki, J.B. Jung, K.P. Hyeon, M.K. Soo, H.Z. Geng, A.P. Kyung, H.J. Shin, S.M. Yoon, A. Benayad, J.Y. Choi, H.L. Young, Fermi level engineering of single-walled carbon nanotubes by AuCl3doping, J. Am. Chem. Soc. (2008). doi:10.1021/ja8038689.

[19] C. Paukner, K.K.K. Koziol, Ultra-pure single wall carbon nanotube fibres continuously spun without promoter, Sci. Rep. (2014). doi:10.1038/srep03903.

[20] B. Yu, C. Liu, P.X. Hou, Y. Tian, S. Li, B. Liu, F. Li, E.I. Kauppinen, H.M. Cheng, Bulk synthesis of large diameter semiconducting single-walled carbon nanotubes by oxygen-assisted floating catalyst chemical vapor deposition, J. Am. Chem. Soc. (2011). doi:10.1021/ja2008278.

[21] W. Ren, F. Li, H.M. Cheng, Evidence for, and an understanding of, the initial nucleation of carbon nanotubes produced by a floating catalyst method, J. Phys. Chem. B. (2006). doi:10.1021/jp062526x.

[22] S.R. St. C., S.W. M., G.A. R., XPS of sulphide mineral surfaces: metal-deficient, polysulphides, defects and elemental sulphur, Surf. Interface Anal. (1999). doi:10.1002/(SICI)1096-9918(199908)28:1<101::AID-SIA627>3.0.CO;2-0.

[23] J.J. Fan, Y.J. Fan, R.X. Wang, S. Xiang, H.G. Tang, S.G. Sun, A novel strategy for the synthesis of sulfur-doped carbon nanotubes as a highly efficient Pt catalyst support toward the methanol oxidation reaction, J. Mater. Chem. A. (2017). doi:10.1039/c7ta05102f.

[24] D.C. Higgins, M.A. Hoque, F. Hassan, J.Y. Choi, B. Kim, Z. Chen, Oxygen reduction on graphene-carbon nanotube composites doped sequentially with nitrogen and sulfur, ACS Catal. (2014). doi:10.1021/cs5003806.

[25] M. Descostes, F. Mercier, N. Thromat, C. Beaucaire, M. Gautier-Soyer, Use of XPS in the determination of chemical environment and oxidation state of iron and sulfur samples: Constitution of a data basis in binding energies for Fe and S reference compounds and applications to the evidence of surface species of an oxidized py, Appl. Surf. Sci. (2000). doi:10.1016/S0169-4332(00)00443-8.

[26] S. AN, The Reaction Mechanisms of H2S Decomposition into Hydrogen and Sulfur: Application of Classical and Biological Thermodynamics, J. Thermodyn. Catal. 08 (2017). doi:10.4172/2157-7544.1000186.

[27] A.N. Startsev, N.N. Bulgakov, S.P. Ruzankin, O. V. Kruglyakova, E.A. Paukshtis, The reaction thermodynamics of hydrogen sulfide decomposition into hydrogen and diatomic

sulfur, J. Sulfur Chem. (2015). doi:10.1080/17415993.2015.1010533.

[28] D.R. Alfonso, First-principles studies of H2S adsorption and dissociation on metal surfaces, Surf. Sci. (2008). doi:10.1016/j.susc.2008.07.001.

[29] L. Zhang, P.X. Hou, S. Li, C. Shi, H.T. Cong, C. Liu, H.M. Cheng, In situ TEM observations on the sulfur-assisted catalytic growth of single-wall carbon nanotubes, J. Phys. Chem. Lett. (2014). doi:10.1021/jz500419r.

[30] J. Wei, H. Zhu, Y. Jia, Q. Shu, C. Li, K. Wang, B. Wei, Y. Zhu, Z. Wang, J. Luo, W. Liu, D. Wu, The effect of sulfur on the number of layers in a carbon nanotube, Carbon N. Y. (2007). doi:10.1016/j.carbon.2007.07.001.

[31] H. Jiang, A.G. Nasibulin, D.P. Brown, E.I. Kauppinen, Unambiguous atomic structural determination of single-walled carbon nanotubes by electron diffraction, Carbon N. Y. (2007). doi:10.1016/j.carbon.2006.07.025.

[32] M.S. Motta, A. Moisala, I.A. Kinloch, A.H. Windle, The Role of Sulphur in the Synthesis of Carbon Nanotubes by Chemical Vapour Deposition at High Temperatures, J. Nanosci. Nanotechnol. (2008). doi:10.1166/jnn.2008.500.

[33] C. Hoecker, F. Smail, M. Pick, L. Weller, A.M. Boies, The Dependence of CNT Aerogel Synthesis on Sulfur-driven Catalyst Nucleation Processes and a Critical Catalyst Particle Mass Concentration, Sci. Rep. (2017). doi:10.1038/s41598-017-14775-1.

[34] Y. Tian, H. Jiang, P. Laiho, E.I. Kauppinen, Validity of Measuring Metallic and Semiconducting Single-Walled Carbon Nanotube Fractions by Quantitative Raman Spectroscopy, Anal. Chem. (2018). doi:10.1021/acs.analchem.7b03712.

[35] F. Yang, X. Wang, D. Zhang, K. Qi, J. Yang, Z. Xu, M. Li, X. Zhao, X. Bai, Y. Li, Growing Zigzag (16,0) Carbon Nanotubes with Structure-Defined Catalysts, J. Am. Chem. Soc. 137 (2015) 8688–8691. doi:10.1021/jacs.5b04403.

[36] Q. Yuan, F. Ding, How a zigzag carbon nanotube grows, Angew. Chemie - Int. Ed. (2015). doi:10.1002/anie.201500477.

[37] B. Liu, J. Liu, X. Tu, J. Zhang, M. Zheng, C. Zhou, Chirality-dependent vapor-phase epitaxial growth and termination of single-wall carbon nanotubes, Nano Lett. (2013). doi:10.1021/nl402259k.

[38] K.K. Kim, S.M. Yoon, H.K. Park, H.J. Shin, S.M. Kim, J.J. Bae, Y. Cui, J.M. Kim, J.Y. Choi, Y.H. Lee, Doping strategy of carbon nanotubes with redox chemistry, New J. Chem. (2010). doi:10.1039/c0nj00138d.

**Graphical abstract**

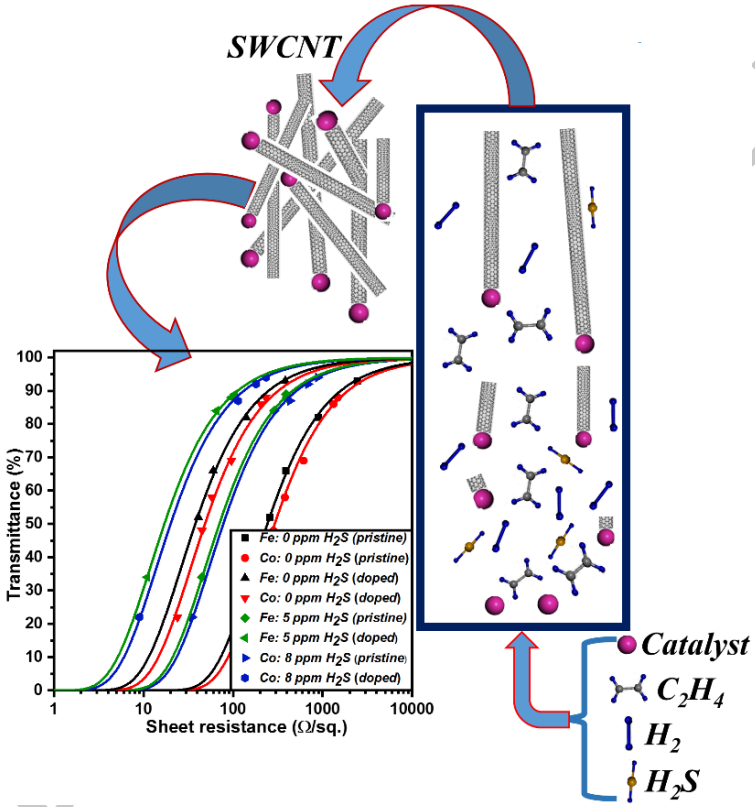

- ✓ Systematically investigated the roles of sulfur on various growth profiles of SWCNTs
- ✓ Sulfur increased the bundle length, SWCNT diameter and performance of SWCNT-TCFs
- ✓ SWCNTs yield is highly sensitive to catalyst composition and sulfur concentration
- ✓ Chirality distributions of SWCNTs was determined by electron diffraction technique